

## Article

# Mass Spectrometry-Based Approach to Compute Electron-Impact Partial Ionization Cross-Sections of Methane, Water and Nitromethane from Threshold to 5 keV

Meetu Luthra <sup>1</sup>, Kanupriya Goswami <sup>2</sup> , Ajay Kumar Arora <sup>2</sup>, Anand Bharadvaja <sup>1,\*</sup>  and Kasturi Lal Baluja <sup>3</sup>

<sup>1</sup> Department of Physics, Bhaskaracharya College of Applied Sciences, University of Delhi, New Delhi 110075, India; meetu.luthra@bcas.du.ac.in

<sup>2</sup> Department of Physics, Keshav Mahavidyalaya, University of Delhi, Delhi 110034, India; kanupriyagoswami@keshav.du.ac.in (K.G.); akarora@keshav.du.ac.in (A.K.A.)

<sup>3</sup> Formerly at Department of Physics and Astrophysics, University of Delhi, Delhi 110007, India; kl\_baluja@yahoo.com

\* Correspondence: anand\_bharadvaja@yahoo.com

**Abstract:** The electron impact partial ionization cross-sections of molecules such as methane, water and nitromethane are computed using a modified form of the binary encounter Bethe (BEB) formula. The modified form of the BEB model works on rescaling the molecular binding energies of the orbitals and the scaling of cross-sections using the electron ionization mass spectrometry data. The computed partial ionization cross-sections are consistent with the recommended data and are better than several experimental and theoretical results. The summed partial ionization cross-sections of different fragments also agree with the total ionization cross-sections obtained from BEB and the experimental data. This work highlights the utility of mass spectrometry in the modeling and interpretation of the ionization cross-section data. The limitations and the advantages of the modified form of the BEB model are also discussed.

**Keywords:** electron collision; ionization cross-sections; BEB model; mass spectrometry; appearance energy; semi-empirical methods; close-coupling methods; differential oscillator strengths



**Citation:** Luthra, M.; Goswami, K.; Arora, A.K.; Bharadvaja, A.; Baluja, K.L. Mass Spectrometry-Based Approach to Compute Electron-Impact Partial Ionization Cross-Sections of Methane, Water and Nitromethane from Threshold to 5 keV. *Atoms* **2022**, *10*, 74. <https://doi.org/10.3390/atoms10030074>

Academic Editors: Dhanoj Gupta, Suvam Singh and Paresh Modak

Received: 30 May 2022

Accepted: 8 July 2022

Published: 14 July 2022

**Publisher's Note:** MDPI stays neutral with regard to jurisdictional claims in published maps and institutional affiliations.



**Copyright:** © 2022 by the authors. Licensee MDPI, Basel, Switzerland. This article is an open access article distributed under the terms and conditions of the Creative Commons Attribution (CC BY) license (<https://creativecommons.org/licenses/by/4.0/>).

## 1. Introduction

The electron impact ionization cross-sections of a molecule and its fragments created due to dissociation are relevant in fields such as low-temperature plasma, radiation chemistry, fusion reactors and plasma processing [1–9]. The cross-sections are also required to model the charge carrier balance in plasma and gas-phase media [10,11]. The ionization rate coefficients of the cations, which are essential in various plasma applications, such as gas discharge and flowing afterglow studies [12], can be obtained using the partial ionization cross-sections. The inter-channel coupling between the discrete spectrum and continuum states, the presence of a large number of channels and the multicenter nature of the molecule make it very difficult to model the scattering phenomenon using the ab initio methods based on the close-coupling (CC) scheme [13]. The ab initio methods such as convergent close coupling [14] and time-dependent close coupling [15] have produced cross-sections due to dissociative and total ionization processes for lighter diatomic molecules and atoms only. The semi-empirical methods, such as the binary encounter dipole (BED) or binary encounter Bethe (BEB) [16], Deutsch and Märk formalism [17] and Khare–Jain model [18], are frequently used to estimate total ionization cross-sections. The modified semi-empirical form of Jain and Khare has been used to compute partial as well as total ionization cross-sections [19–21]. Both the BED and modified Jain and Khare models have differential dipole oscillator strength as the key input parameter. This quantity is always challenging to obtain and has thus limited the wider applicability of both these models. On the other hand, the BEB model is independent of the differential oscillator

strength and has several other advantages, e.g., it does not require knowledge of the bound or continuum wave functions and fitting parameters. Moreover, the BEB cross-section has a very simple analytical form. The total ionization cross-sections in the BEB model are obtained using input parameters such as the occupation number, binding energy and kinetic energies of the occupied orbitals, which are easily obtained from quantum chemical software. This makes the BEB model very simple to use in comparison to other methods. Moreover, the BEB model has satisfactorily reproduced the experimental total ionization cross-sections of many molecules over a wide energy range and for different quantum chemical approaches [22–26].

However, the BEB model cannot be applied to estimate ionization cross-sections of fragments produced either due to ionization or dissociative ionization processes. In the present work, we have modified the BEB model and investigated its efficacy by computing partial ionization cross-sections of molecules such as methane, water and nitromethane. Nitromethane, in comparison to the other two molecules, has a significantly large number of ionic species. The results obtained from the modified BEB (m-BEB) model are consistent with the experimental results for all three targets considered. The work establishes a close link between the modeling of ionization cross-sections and electron mass spectrometry. It also addresses the vital issue of the applicability of the BEB model for computing partial ionization cross-sections [27].

While there are multiple advantages of the modified BEB model, there are inherent limitations as well. Similar to the BEB model, this model cannot provide details of resonances in the continuum, vibrational and/or rotational excitations. The partial ionization cross-sections due to doubly, triply, etc., ionized cations and the cations formed due to multi-pathways, post-ionization collisions or transition-state pathways are not possible to account for. The present mass spectrometry-based BEB approach is novel and is aimed at providing an extremely easy procedure to compute the partial ionization cross-sections of ions that may otherwise be not possible to calculate even with expensive computational resources. The modified BEB model would certainly be useful in plasma modeling, plasma processing and in fields such as atmospheric and radiation physics, etc., where partial cross-sections are required. The salient features of the BEB and modified BEB models are presented in Section 2. The results are presented in Section 3, and the conclusion is drawn in Section 4.

## 2. The BEB and Modified BEB Models

### 2.1. The BEB Model

The analytical form of the BED or BEB models proposed by Kim and Rudd [16] is a combination of Mott's and Bethe's scattering. The hard collisions are described by Mott theory and soft collisions are described by Bethe theory. These models calculate the electron-impact ionization cross-sections of the ground-state atoms and molecules as a function of incident energy by using only the bound-state properties of the target, without explicitly using continuum functions. In the BED model [16], the total ionization cross-section,  $\sigma^{(I)}$ , due to electron impact for any target, is the sum of the ionization cross-section over bound molecular orbitals  $i$ :

$$\sigma_{BED}^I(t) = \sum_i \frac{S_i}{t_i + (u_i + 1)/n} \left[ \frac{Q}{2} \left( 1 - \frac{1}{t_i^2} \right) \ln t_i + (2 - Q) \left\{ \left( 1 - \frac{1}{t_i} \right) - \frac{\ln t_i}{t_i + 1} \right\} \right] \quad (1)$$

where  $t_i = E/B_i$ ,  $u_i = U_i/B_i$  are the reduced incident and orbital kinetic energy, respectively, and  $S_i = 4\pi a_0^2 N_i (R/B_i)^2$ . The notations  $E$ ,  $R$  and  $a_0$  refer to the incident energy of the projectile, Rydberg constant and Bohr's radius, respectively.  $B_i$ ,  $U_i$  and  $N_i$  are the magnitude of the binding energy, orbital kinetic energy and the occupancy number of the  $i$ th orbital, respectively. The constant  $n$  is the principal quantum number of the dominating atomic orbitals, which may contribute significantly to the total ionization cross-sections [28–30]. The choice of threshold to put  $n \geq 3$  is arbitrary [31]. The  $\sigma_{BED}^I = 0$  if the incident electron

does not have enough energy to ionize the orbital, i.e.,  $E < B$ . The quantity  $Q$  is related to continuum oscillator strength.

Although both Mott and Bethe cross-sections have  $t$  dependence, in the BED model,  $t$  is replaced by  $(t + u + 1)$  [32] to make the incident electron equivalent to the target electron. This form of energy scaling is without any proper derivation and is different for ions [33,34] and K-shell ionization cross-sections [24]. It may be noted that the term  $(t + u + 1) \rightarrow t$  in the Born approximation.

Using  $Q = 1$  in Equation (1) has undoubtedly simplified the BED model as differential oscillator strengths construe a bottleneck in the calculations. The substitution of  $Q = 1$  in the BED model describes the well-known BEB model for total ionization cross-sections [16].

The BEB model requires inputs such as  $B$ ,  $U$  and  $N$  for different molecular orbitals to compute total ionization and partial ionization cross-sections. These parameters can be obtained using quantum chemical software at different levels of theory, such as Hartree–Fock (HF), Density Functional Theory (DFT), etc., and different basis sets. The effective core potentials (ECP) can also be used to generate input parameters [22,23,28,29,35–38]. The ECP approach is better suited to heavier atoms or molecules consisting of heavier atoms. The total ionization cross-sections at a particular theory level are insensitive to moderate- and good-quality basis sets but are highly sensitive to the binding energy of the valence molecular orbital. For this reason, the experimental value for the ionization energy (IE) of the outermost electron is always preferred since it is the most dominating orbital in its contribution to total ionization cross-sections [28]. This also ensures the correct threshold behavior of cross-sections. The deep inner shells have a very high binding energy and thus do not participate in the ionization process. The BEB results are generally within 15–20% of the experimental results at the peak value of the cross-section irrespective of the theoretical approach. Being a semiempirical approach to computing ionization cross-sections, there is no fixed rule that the inputs need to be calculated from sophisticated correlated methods or large basis sets. The HF models have yielded fairly good ionization cross-sections for many molecules using the moderate basis sets [25,26,29].

## 2.2. The Modified BEB Model

As the incident energy of the electron exceeds the ionization threshold, the target is fragmented into positively charged ions via the dissociative ionization (DI) process. Since the cations are characterized by appearance energies ( $AE$ ) and not by ionization energy (IE), the first step to building the BEB model for the DI process is to transform  $B$  in such a way that the energy of the highest occupied molecular orbital (HOMO) becomes the  $AE$  of the cation in Equation (1) with  $Q = 1$ . The  $AE$  for any cation is always higher than  $B$ , and a transformation such as  $B \rightarrow \Delta + B$  in Equation (1) for all MO seems justified. Here,  $\Delta = AE - IE$ . Thus, for fragment  $j$ ,  $t_j = E/(B_j + \Delta_j)$ ,  $\Delta_j = AE_j - B_j$ .

Once the energy transformation is applied to Equation (1), the partial ionization cross-sections are multiplied by a normalization constant. This ensures that the m-BEB model provides the branching ratios (BR), which are normalized to the experimental values and also satisfy the condition that their sum over different fragments  $j$  becomes unity at a particular energy. The expression for the partial ionization cross-sections for a cation  $j$  in the modified BEB model, after incorporating the above modifications, is given by

$$Q'_j(t) = \Gamma_j \sum_i \frac{S_{ji}}{t_{ji} + u_{ji} + 1} \left[ \frac{1}{2} \left( 1 - \frac{1}{t_{ji}^2} \right) \ln t_{ji} + 1 - \frac{1}{t_{ji}} - \frac{\ln t_{ji}}{t_{ji} + 1} \right] \quad (2)$$

Here,  $t_{ji} = E/(B_{ji} + \Delta_{ji})$ , and  $S_{ji} = 4\pi a_0^2 N_i (R/t_{ji})^2$ . The quantities with subscript  $j$  in Equation (2) refer to cation parameters;  $\Gamma_j$  represents the normalized constant. The normalization constant can be obtained using the mass spectrometry data. The details can be sought in our earlier paper [39].

### 3. Methodology and Computational Details

The input parameters to compute BEB cross-sections were obtained at the optimized geometry [40] carried out at the HF level using Gaussian 03 software [41]. All targets are closed-shell molecules having doubly occupied orbitals. The experimental values of IE and AE were used to ensure the correct threshold behavior of the total ionization cross-sections and partial ionization cross-sections, respectively, for reasons mentioned earlier. Since there are no pure theoretical methods for predicting the relative intensities of fragment ions [42], the energy-specific BR were obtained either from the cross-section data or electron ionization mass spectrometry (EIMS) data. The present work focuses on EIMS data to obtain partial ionization cross-sections within the BEB formulation. Hence, for comparison purposes, we have considered the recommended data and experimental values of partial ionization cross-sections. Towards the end, some aspects of the modified form of the BEB model are discussed. Here, we discuss the three targets in detail.

#### 3.1. Methane ( $\text{CH}_4$ )

Methane is the simplest hydrocarbon molecule, with relevance in the field of technology and atmospheric studies. Its electron impact ionization cross-sections are required to understand the planetary atmospheres [43–45] and plasma processing [46]. The work of Gadoum et al. is the latest on electron–methane collision. They have determined a set of electron collision cross-section data for methane [47]. Song et al. [48] have recommended the database of Lindsay and Mangan [49] within the uncertainty of  $\pm 5\%$  for total ionization cross-sections and  $\pm 10\%$  for partial ionization cross-sections. Lindsay and Mangan [49] recalibrated and corrected the data of Straub et al. [50] by taking into account the production of positive ion pairs. Straub et al. [50] performed the measurements at 200 eV electron energy. The EIMS data of methane recorded at 70 eV are available from the NIST Chemistry WebBook database [51] and were used to obtain the BR for different cations. Both the NIST-EIMS spectra [51] and Straub et al.'s [50] cross-section data predict the parent ions  $\text{CH}_4^+$  and  $\text{CH}_3^+$  as the dominating species but they differ in their contribution to total ionization cross-sections. The NIST mass spectra predict their respective contributions to be around 44% and 40%, whereas the corresponding estimates from the measurements of Straub et al. [50] are 41% and 34%, respectively. This difference in the contribution is a reflection of the relative cation intensity (RI) data. The NIST-EIMS database [51] reports cations having nominal masses from 12 to 16. All experimental groups and recommended data have also included lighter ions such as  $\text{H}^+$  and  $\text{H}_2^+$  in their measurements, in addition to cations with  $m/z = 12$  to 16. According to the measurements provided by Straub et al., the contribution of the  $\text{H}^+$  is approximately 10%, whereas the  $\text{H}_2^+$  makes an insignificant contribution to the total ionization cross-sections [50].

In this work, for computing the partial ionization cross-sections, the AE recommended by Song et al. [48] were used. The normalization constant  $\Gamma$  was obtained using the EIMS data available from the NIST Chemistry WebBook database [51]. The  $B$  and  $U$  for different orbitals were obtained using the D95\*\* basis set.

The partial ionization cross-sections obtained from the m-BEB model are displayed in Figures 1a, 2a and 3a. The total ionization cross-sections from the BEB model are shown in Figure 3b. The higher estimates of partial ionization cross-sections from the m-BEB model are due to the cumulative effect of the EIMS data of the channels and the overestimated BEB results. The expected deviation between the m-BEB model results, experimental and the recommended data is 15%. To minimize the impact of the overestimated BEB results (Figure 3b) on the m-BEB data, we normalized the BEB ionization cross-section data [52] to the recommended data of Song et al. [48]. The calculations of partial ionization cross-sections were redone with the normalized BEB data. This substantially reduced the earlier results and brought the m-BEB results closer to the recommended data of Song et al. [48]. Since the NIST-EIMS data do not include channels such as  $\text{H}^+$  and  $\text{H}_2^+$ , a further reduction in the m-BEB (normalized) cross-sections would happen on the inclusion of these channels in the computation. It has been noted in experimental studies [53] and

shown theoretically [54] that the exclusion of channels overestimates the partial ionization cross-section results.

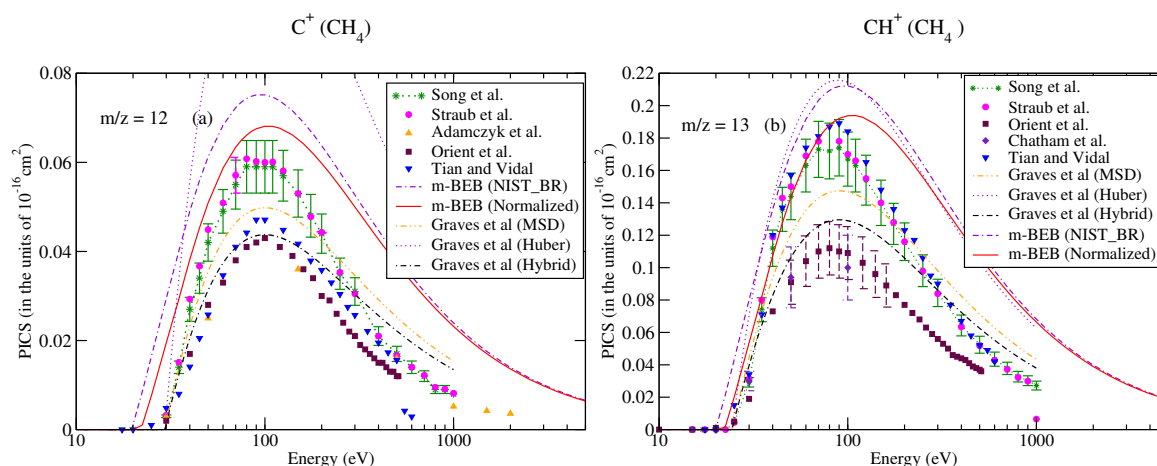


**Figure 1.** Partial-ionization cross-sections for different fragments of methane: (a)  $m/z = 12$ , (b)  $m/z = 13$ . Line curve, m-BEB (normalized); dashed curve, m-BEB (using NIST mass spectrometry data); double dots with dashed curve, Graves et al. [26] from MSD model; dots, Graves et al. [26] from Huber model; dots with dashed curve; Graves et al. [26] from hybrid model; triangles inverted, Tian and Vidal [45]; recommended data of Song et al. [48]; dots with star, circles, experimental data of Straub et al. [50]; triangles, Adamczyk et al. [55]; squares, Orient et al. [56]; diamonds, Chatham et al. [57].

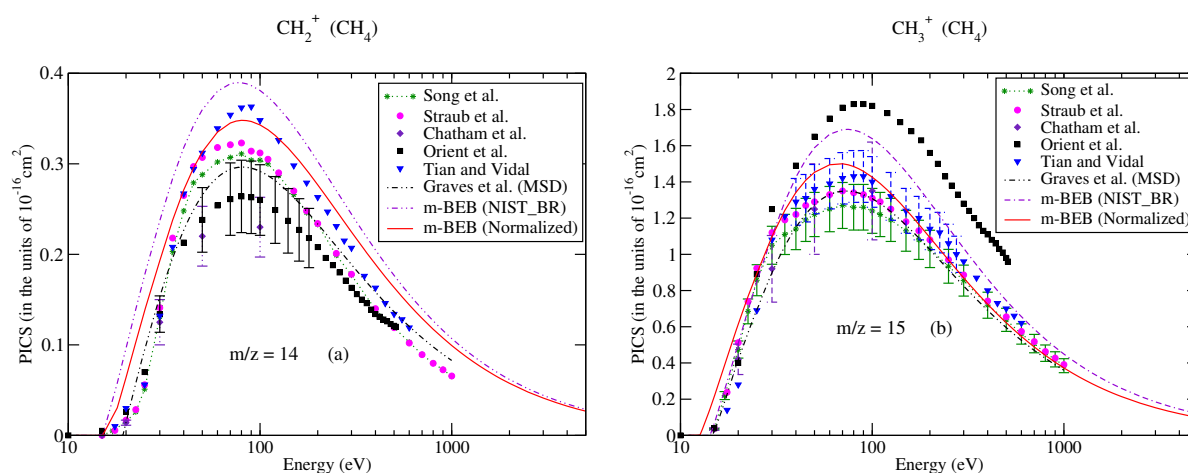


**Figure 2.** Caption same as Figure 1 but for (a)  $m/z = 14$ , (b)  $m/z = 15$ .

Since the present results are sensitive to the BR and AE of the cations, and to bring more clarity to the present work, we have compared the BR of different cations obtained from the recommended cross-section data of Song et al. [48] and the NIST Chemistry WebBook database [51]. This comparison is shown in Table 1. It is apparent that the variations in BR obtained from Song et al.’s [48] cross-section data and the NIST mass spectrometry data [51] are one of the reasons for the difference arising in the m-BEB (normalized) results. A renormalization of Song et al.’s [48] channel data increases the value of BR for each cation and brings it closer to the corresponding values obtained from NIST mass spectrometry data [51]. This also suggests that the higher estimates of the partial ionization cross-sections from m-BEB (normalized) are largely due to the exclusion of two lighter channels,  $H^+$  and  $H_2^+$ , in the NIST mass spectrometry data [51].

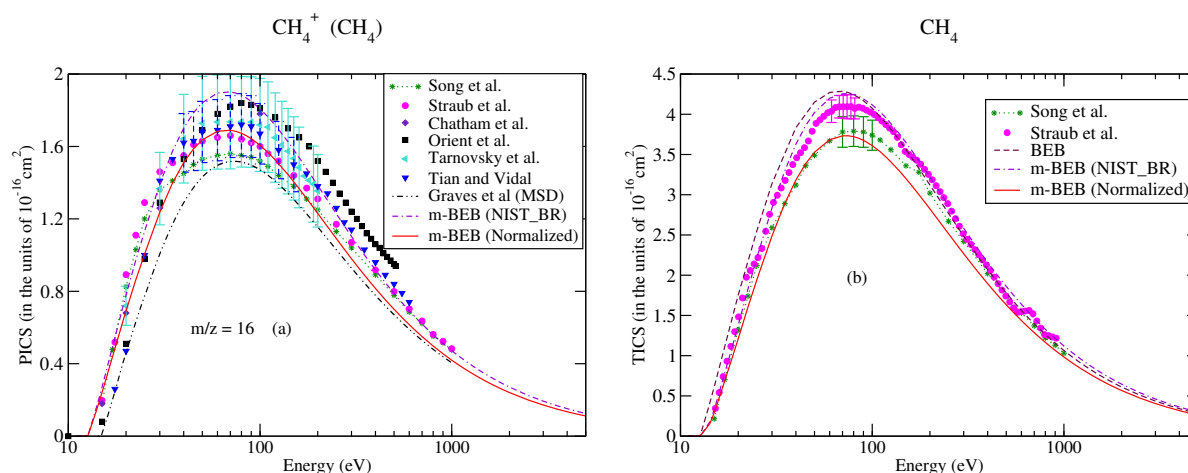


**Figure 3.** Caption same as Figure 1 for (a)  $m/z = 16$ ; triangles left, Tarnovsky et al. [58], (b) total ionization cross-sections.

**Table 1.** Branching ratios (BR) of various cations of methane produced by electron impact dissociation at 70 eV.

Ions	$m/z$	Song et al. ‡ [48]	NIST Chemistry WebBook Database [51]	Song et al. ‡ (Renormalized) [48]
$\text{H}^+$	1	0.10053	-	-
$\text{H}_2^+$	2	0.9260 (-2) *	-	-
$\text{C}^+$	12	0.1455 (-1)	0.1699 (-1)	0.1634 (-1)
$\text{CH}^+$	13	0.4577 (-1)	0.4779 (-1)	0.5141 (-1)
$\text{CH}_2^+$	14	0.8122 (-1)	0.9129 (-1)	0.9123 (-1)
$\text{CH}_3^+$	15	0.3360	0.3967	0.3774
$\text{CH}_4^+$	15	0.4127	0.4470	0.4636

‡ recommended ionization cross-section data. \* The notation (-n) signifies  $\times 10^{-n}$ .

It is well known that cross-sections or RI are difficult to measure accurately for lighter fragments [53]. The large uncertainties in the measurements of RI in  $\text{H}^+$  and  $\text{H}_2^+$  ions might be one of the reasons for the exclusion of these channels in the NIST mass spectrometry database [51]. To bring completeness to the present work, we have also estimated the partial ionization cross-sections for  $\text{H}^+$  and  $\text{H}_2^+$  ions (shown in Figure 4). This was also a test to assess the effectiveness of the m-BEB method for lighter ions. The BR for these ions were calculated using the cross-section data of Song et al. [48]. The predictions of the m-BEB model for  $\text{H}^+$  and  $\text{H}_2^+$  ions do not appear attractive at energies away from the main peak as there is a significant deviation in the results from the experimental results. This deviation is because the formation of the  $\text{H}^+$  ion in methane happens due to multiple pathways [59] and corresponds to a large energy barrier. These features are not included in this model. Thus, the m-BEB model may not deal efficiently with the problem of scattering of the point charges.

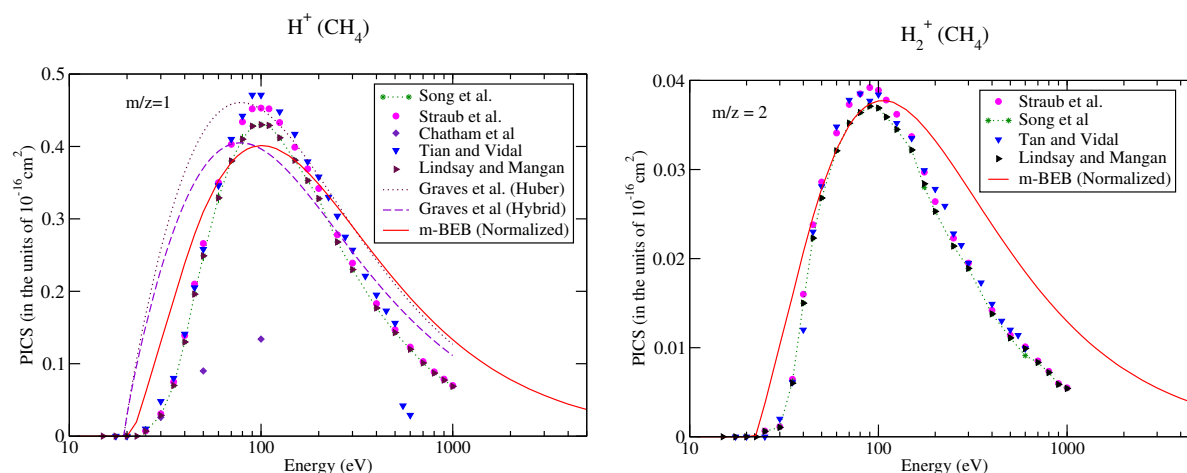


**Figure 4.** Caption same as Figure 1 but for (a)  $m/z = 1$ , (b)  $m/z = 2$ . Line curve, m-BEB; Graves et al. [26] from Huber model; dots with dashed curve; Graves et al. [26] from hybrid model; triangles inverted, Tian and Vidal [45]; dots with star, recommended data of Song et al. [48]; dots, circles, experimental data of Straub et al. [50]; diamonds, Chatham et al. [57]; triangles, Lindsay and Mangan [60].

It is worth comparing the present results with the recent theoretical results of Graves et al. [26]. Graves et al. [26] multiplied the total ionization cross-sections computed from the BEB model with the BR of a cation to calculate its partial ionization cross-sections. The BR was obtained by these authors from the experimental NIST mass spectrometry database [51] directly (similar to us) but with a different approach. They also invoked two more models, namely the Huber [38] and hybrid models, to obtain the BR. The authors presented their results only for the  $H^+$  ion using the Huber and hybrid models. Their results from the hybrid model are closer to the m-BEB results in shape and magnitude. The only difference is that there is a shift in the peak of the cross-section curve to a slightly lower energy. The Huber model estimates are higher. This shift in the peak of the curve to a lower energy value is due to the lower value of AE (19.24 eV) used by them in their theoretical calculations. We have taken the AE of the  $H^+$  ion as 21.1 eV [48]. Overall, the present results are consistent with the work of Graves et al. [26].

### 3.2. Water ( $H_2O$ )

Water is the third most abundant molecule in the Universe after  $H_2$  and CO [61] and the main product of the combustion of hydrocarbon fuels. Hence, it is one of the essential ingredients of the model flue gas. The electron–water interactions are highly significant in astrophysics [62,63], medicine [64–66], low-temperature plasma techniques to control pollution from fossil fuel combustion [67], radiation damage [68] and many other related fields. Several electron impact ionization studies have been performed for water [69–73]. Lindsay and Mangan [60] recommended the electron impact ionization cross-sections on the basis of the measurements done by Straub et al. [70] at 100 eV. Song et al. [74] and Itikawa et al. [75] recommended the Lindsay and Mangan [60] values of ionization cross-sections for water.

The NIST-EIMS recorded at 70 eV [51] has reported only three fragments corresponding to mass to charge ratios of 16, 17 and 18. Straub et al. [70] recorded their observations at 100 eV but have reported two additional ions,  $H^+$  and  $H_2^+$ .

We obtained the BR using the recommended data of Song et al. at the very energy at which the mass spectrum was recorded by Straub et al. [70]. This was done to include contributions of all channels to the total ionization cross-sections. The parent ion  $H_2O^+$  is the most dominating cation. The cations such as  $H_2O^+$ ,  $OH^+$  and  $H_2^+$  contribute around 60%, 20% and 16%, respectively, to the total ionization cross-sections. The NIST-EIMS database [51] provides significantly higher estimates of  $H_2O^+$  around 82% and comparable

estimates of  $\text{OH}^+$  cations around 16% to the total ionization cross-sections. The partial ionization cross-sections obtained from RI data have higher values due to neglecting a few channels, as pointed out in the case of methane.

The values of  $B$  and  $U$  for occupied orbitals were obtained using the D95\*\* basis set. The values of AEs of cations were derived from different sources [51,75]. The total ionization cross-sections obtained from the BEB model were higher than the recommended values of Song et al. [74] by less than 8%. This issue has been explained by Song et al. [74] in their review paper. It means that the present m-BEB model is bound to yield results of higher amplitudes. We, therefore, normalized the BEB cross-sections to the results of Song et al. [74] at 100 eV. The normalized total ionization cross-sections and partial ionization cross-sections are shown in Figures 5–8. The partial ionization cross-sections obtained from the m-BEB model renormalizing the BEB data show excellent agreement with the recommended data of Song et al. [74] and are better than the experimental works of King et al. [76] and Montenegro et al. [77]. Only the scaled ionization cross-sections of Montenegro et al. [77], as suggested by Song et al. [74], showed agreement with the present results. These are also displayed in Figures 5–8.

For the sake of a better understanding of the model, we have also shown the partial ionization cross-sections obtained using the unnormalized BEB data.

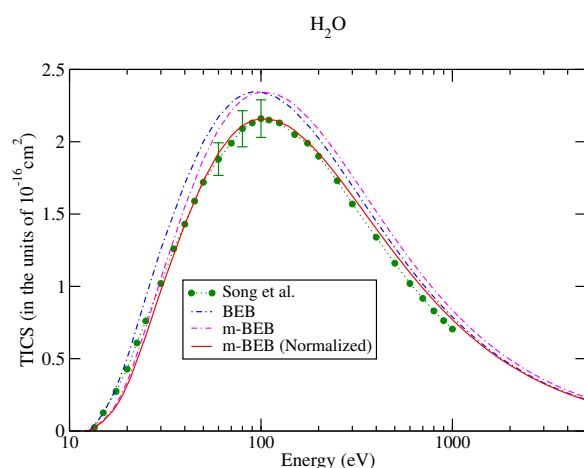


**Figure 5.** Total ionization cross-sections of water: dots with circles, recommended data of Song et al. [74]; BEB model, dashed dotted curve, m-BEB model, dashed dotted curve; line curve, normalized m-BEB model.

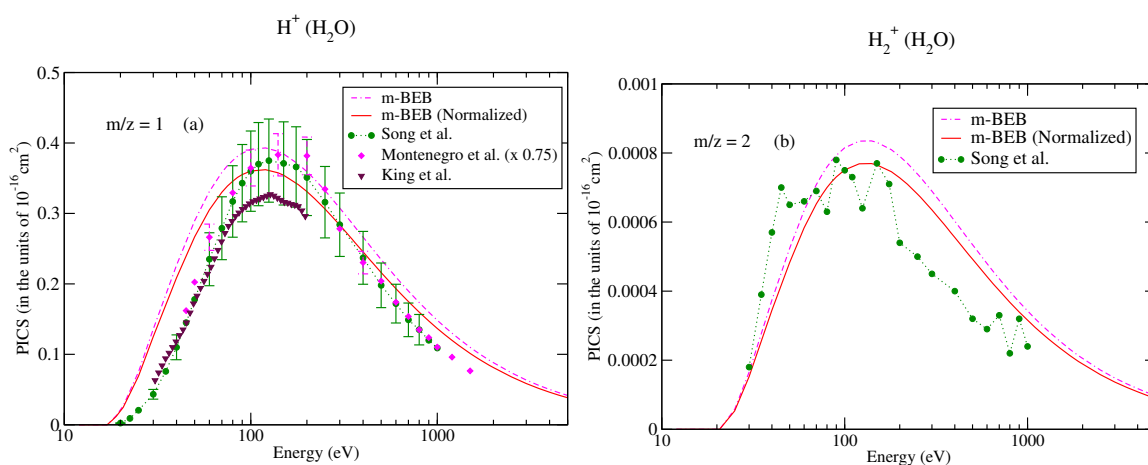


**Figure 6.** Partial ionization cross-sections for different fragments of water: (a)  $m/z = 1$ , (b)  $m/z = 2$ . dashed dotted curve, m-BEB; line curve, normalized m-BEB; dots with circles, recommended data of Song et al. [74]; inverted triangles, King et al. [76]; diamonds, scaled cross-sections of Montenegro et al. [77].

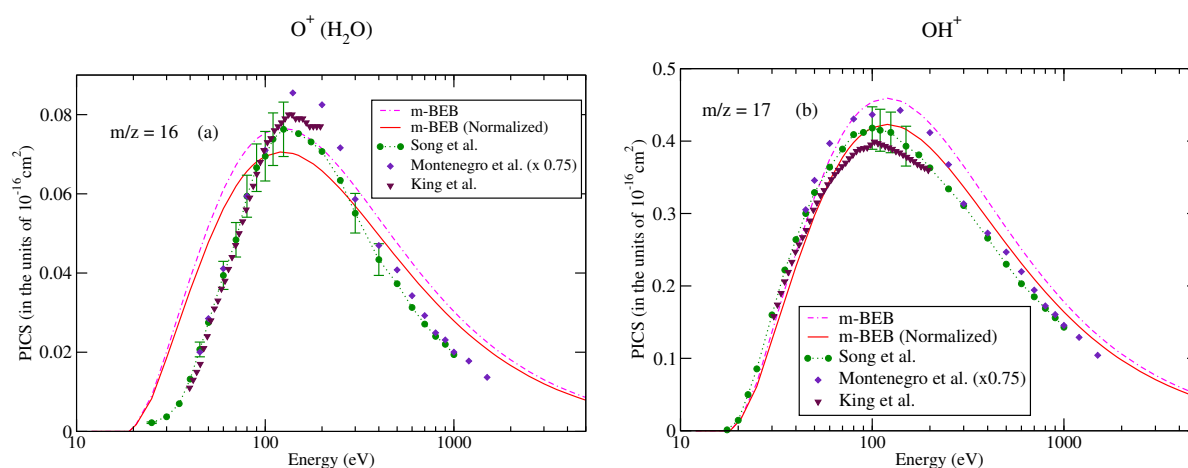


**Figure 7.** Caption same as Figure 5 but for (a)  $m/z = 16$ , (b)  $m/z = 17$ .

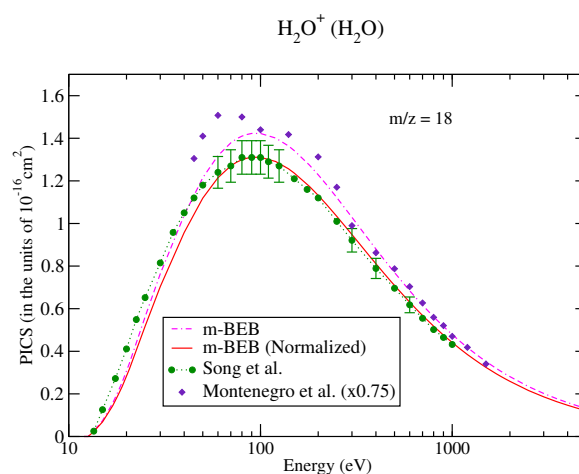


**Figure 8.** Caption same as Figure 5 but for  $m/z = 18$ .

### 3.3. Nitromethane ( $CH_3NO_2$ )

The nitro-organic compounds have significant potential for industrial use as an explosive [78–82], propellant [83–85] and high-performance fuel additives for detonation systems and combustion engines [86,87]. This molecule serves as a model system for studying biological surface science as it contains functional groups such as  $NO_2$  and  $CH_3$ , which show significant biological activity [88]. Thus, it has relevance in fields such as medical implants, bio-sensors and bio-chips for diagnostics, tissue engineering and bio-electronics [89]. For use as a fuel, an efficient design of plasma-assisted ignition engines is required, which in turn requires a comprehensive database of the electron-impact ionization cross-sections of the fragments. Jiao et al. [90] used Fourier transform mass spectrometry (FTMS) to measure absolute DI cross-sections from threshold to 200 eV. These authors detected 13 ions, including the parent ion  $CH_3NO_2^+$  and the four most important fragment ions  $CH_3NO^+$ ,  $NO_2^+$ ,  $NO^+$  and  $CH_3^+$ . Their fragmentation patterns are largely in agreement with NIST-EIMS data [51], except that significantly fewer yields of the parent ion were observed. This is the only available work for the electron ionization of nitromethane.

The ions with low intensities having cross-sections  $<10^{-18}$   $cm^2$  at 70 eV were not included in the FTMS results. The collective contribution of parent ion  $CH_3NO_2^+$  and four major fragments was nearly 76% according to the NIST Chemistry WebBook database [51], 80% as per Kandel [91] and 83% as per Jiao et al. [90] to the total ionization cross-sections.

We have obtained the BR for different fragments using the RI data recorded by the NIST mass spectrum at 70 eV. The ion energetic data were derived from Kandel [91] and the NIST Chemistry WebBook database [51]. The BEB input parameters were obtained at the optimized geometry using the cc-pVTZ basis set.

The digitalized data of Jiao et al. [90] were used to perform a comparison with the present results, as shown in Figures 9 and 10. The m-BEB results obtained using EIMS data are also plotted in the same figures. The partial ionization cross-sections are close to the experimental results of Jiao et al. [90]. The total ionization cross-sections are displayed in Figure 11. The maximum value of the experimental total ionization cross-sections is  $6.8 \text{ \AA}^2$  at 60 eV. The BEB model predicts the maximum cross-section of  $6.6 \text{ \AA}^2$  at 110 eV. At 60 eV, the BEB total ionization cross-sections have a value of  $5.95 \text{ \AA}^2$ . The BEB value lies within the estimated error of 15%. In Figure 11, we have also plotted the estimates of total ionization cross-sections obtained from different models and experimental measurements of Jiao et al. [90]. There is good agreement in the results, thus reflecting the correctness of this methodology.

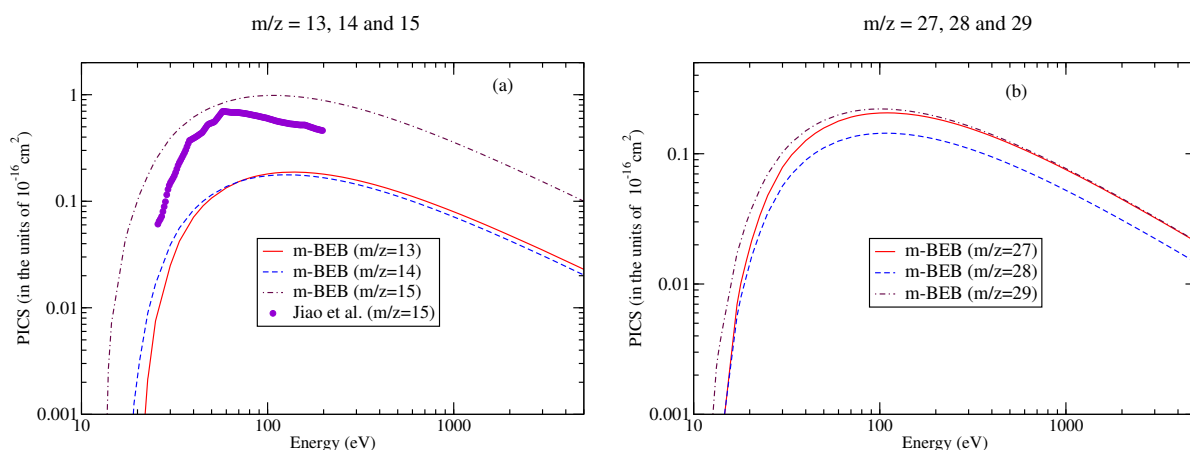


**Figure 9.** Partial ionization cross-sections for different fragments of nitromethane [90] for (a)  $m/z = 13\text{--}15$ , (b)  $m/z = 27\text{--}29$ .

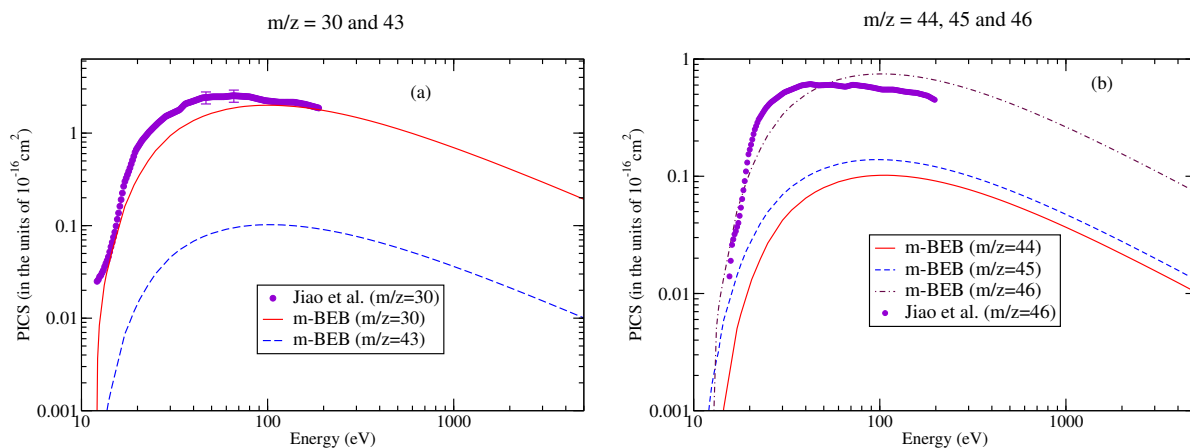


**Figure 10.** Caption same as Figure 9 for (a)  $m/z = 30, 43$ , (b)  $m/z = 44\text{--}46$ .

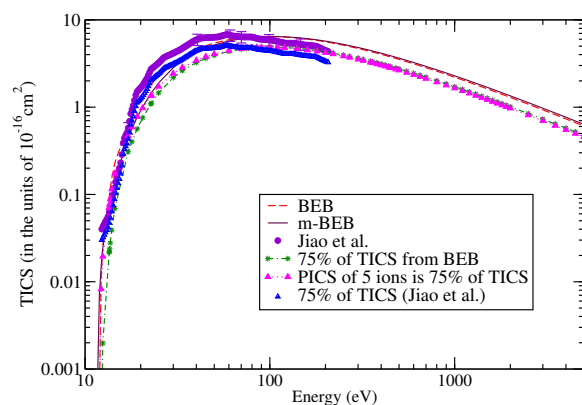


**Figure 11.** Total ionization cross-sections of nitromethane: dashed curves, BEB; line curves, m-BEB; circles, Jiao et al. [90].

We have applied the modified BEB model to obtain partial ionization cross-sections of different fragments in a straightforward and efficient manner. To make the present model predictive, we have made use of EIMS data. The theoretical computations of partial ionization cross-sections are dependent on factors such as ion energetics and relative cation yield data. The success of the BEB model is due to the form of scaling used. It is a well-established fact that the term  $(t + u + 1)$  works very well for molecules only and not cations. We, therefore, modified the BEB model by introducing a fragment-specific scaling term for each cation without altering the simplicity of the BEB model. It corrects the  $(t + u + 1)$  form in the denominator of Equation (2) for cations, thereby producing the correct amplitudes of the cross-sections. The  $\Gamma$  is thus a simple factor that normalizes the theoretical BR to an absolute scale. The present scaling approach eliminates the complexity involved in identifying the correct form of scaling term. Thus, this term has added flexibility to the BEB model in extending its applicability to DI.

Another aspect of this study is energy scaling. The AE are always higher than the IE. A uniform increment to B in the BEB model helped to include the contribution of all MOs to the partial ionization cross-sections. In contrast to *ab initio* methods or differential oscillator strength-based approaches, the present approach does not suffer from any restriction and can be easily applied to any molecule. It also serves as a test to check the consistency of experimental and theoretical data as well as EIMS data, which may be erroneous [92]. The higher partial ionization cross-sections from the modified BEB model are only due to higher ion abundance data, which may be due to the omission of channels. It in no way reflects the shortcoming of the present model. The choice of scaling using BR in the modified BEB is arbitrary. The mass spectrum of the fragmentation pattern is sensitive to the energy of the incoming electron only at low energies, whereas it is stable between 50 eV and 100 eV [93]. In this energy range, the total ion yield is maximum. For this reason, the mass spectrum analysis is done at 70 eV [94]. The availability of ion yield data for many molecules from the NIST Chemistry WebBook database [51] gives an additional advantage in modeling the ionization phenomenon.

This work demonstrates that a simple modification in the BEB model and the magnitude of cross-sections by electron ionization mass spectrometry data provides reliable partial ionization cross-sections of an ion. The use of mass spectrometry data makes the modified BEB model predictive in nature. Undoubtedly, the modified BEB approach may require further refinements, but it at least fills the void and provides a tool for theoretical physicists and experimentalists to obtain and predict partial ionization cross-sections over a wide energy range for which the experimental data were previously unavailable.

The study reveals that the partial cross-sections corresponding to dominant channels where there is a direct ionization or if the energy barrier is small can be estimated with a higher degree of agreement than those channels where indirect processes contribute to the partial ionization cross-sections or the energy barrier is large (especially lighter

ions). However, in the absence of results either from theoretical *ab initio* methods or from experiments, the proposed semiempirical approach, with very limited resources, can predict or provide trends in the partial ionization cross-sections with reasonable accuracy and correct orders of magnitude. The study highlights the need to include all the channels in the mass spectrometry data for better values of partial ionization cross-sections.

#### 4. Conclusions

The partial ionization cross-sections are intrinsic molecular properties and the BEB is a semiempirical approach to compute single electron impact total ionization cross-sections. The cross-section data of reactive species and their fragments are critical for understanding their generation in plasma reactors and other fields. The present m-BEB model is essentially focussed on rescaling the molecular binding energies of the orbitals so as to obtain the correct appearance energy for a particular cation corresponding to neutral target geometry. Mass spectrometry data provide the correct contribution of each ion to the total ionization cross-sections at a particular energy. The theoretical results appear in good agreement with the experimental results, without having to consider the intramolecular chemical processes involved. The present approach has a lot of advantages as it retains all the features that have made the BEB approach popular. The work emphasizes the need to report the values of relative cation abundances along with the partial ionization cross-sections. The results may motivate experimentalists and the partial ionization cross-sections can be used in mass spectrometric plasma diagnostics.

**Author Contributions:** Conceptualization, supervision, methodology, K.L.B. and A.B.; original calculations and draft, A.K.A.; review, calculation checking, redrafting and editing, M.L. and K.G. All authors contributed equally to this work. All authors have read and agreed to the published version of the manuscript.

**Funding:** This research received no external funding.

**Institutional Review Board Statement:** Not applicable.

**Informed Consent Statement:** Not applicable.

**Data Availability Statement:** Can be obtained from the authors on request.

**Conflicts of Interest:** The authors declare no conflict of interest.

**Sample Availability:** Not applicable.

#### Abbreviations

The following abbreviations are used in this manuscript:

BEB	binary encounter Bethe
m-BEB	modified BEB
HF	Hartree–Fock
DFT	Density Functional Theory
ECP	Effective Core Potentials
EIMS	Electron Ionization Mass Spectrometry
DI	Dissociative Ionization
AE	Appearance Energy
IE	Ionization Energy
CC	Close Coupling
$m/z$	mass to charge ratio
eV	electron volt
au	atomic unit
RI	Relative Cation Intensity
BR	Branching Ratios

## References

1. Janev, R.K. (Ed.) *Atomic and Molecular Processes in Fusion Edge Plasmas*; Plenum New York: New York, NY, USA, 1995.
2. McMaster, M.C.; Hsu, W.L.; Coltrin, M.E.; Dandy, D.S.; Fox, C. Dependence of the gas composition in a microwave plasma-assisted diamond chemical vapor deposition reactor on the inlet carbon source:  $CH_4$  versus  $C_2H_2$ . *Diam. Relat. Mater.* **1995**, *4*, 1000. [[CrossRef](#)]
3. Moos, H.W.; Clark, J.T. Detection of acetylene in the Saturnian atmosphere using the IUE satellite. *Astrophys. J.* **1979**, *229*, L107. [[CrossRef](#)]
4. Owen, T.C.; Caldwell, J.; Rivolo, A.R.; Moore, V.; Lane, A.L.; Sagan, C.; Hunt, H.; Ponnampuruma, C. Observations of the spectrum of Jupiter from 1500 to 2000 Å with the IUE. *Astrophys. J.* **1987**, *236*, 139. [[CrossRef](#)]
5. Christophorou, L.G. (Ed.) *Electron Molecule Interactions and Their Applications*; Academic Press: Cambridge, MA, USA, 1984.
6. Christophorou, L.G.; Olthoff, J.K. *Fundamental Electron Interactions with Plasma Processing Gases*; Springer: Boston, MA, USA, 2004.
7. Märk, T.D.; Dunn, G.H. (Eds.) *Electron Impact Ionization*; Springer: Berlin/Heidelberg, Germany, 1985.
8. Pitchford, L.C.; McKoy, B.V.; Chutjian, A.; Trajmar, S. (Eds.) *Swarm Studies and Inelastic Electron-Molecule Collisions*; Springer: New York, NY, USA, 1987.
9. Mohr, J.P.; Wiese, W.L. (Eds.) *Atomic and Molecular Data and their Applications*; AIP Conference Proceedings; AIP: Woodbury, NY, USA, 1998; Volume 434.
10. Morgan, W.L. A critical evaluation of low-energy electron impact cross sections for plasma processing modeling. II:  $Cl_4$ ,  $SiH_4$ , and  $CH_4$ . *Plasma Chem. Plasma Process.* **1992**, *12*, 477. [[CrossRef](#)]
11. PKae-Nune; Perrin, J.; Guillon, J.; Jolly, J. Mass spectrometry detection of radicals in  $SiH_4$ - $CH_4$ - $H_2$  glow discharge plasmas. *Plasma Sources Sci. Technol.* **1995**, *4*, 250. [[CrossRef](#)]
12. Capitelli, M.; Celiberto, R.; Cocciatore, M. Needs for Cross Sections in Plasma Chemistry. *Adv. At. Mol. Opt. Phys.* **1994**, *33*, 321.
13. Ratnavelu, K.; Brunger, M.J.; Buckman, S.J. Recommended Positron Scattering Cross Sections for Atomic Systems. *J. Phys. Chem. Ref. Data* **2019**, *48*, 023102. [[CrossRef](#)]
14. Zammit, M.C.; Fursa, D.V.; Savage, J.S.; Bray, I. Electron- and positron-molecule scattering: Development of the molecular convergent close-coupling method. *J. Phys. B At. Mol. Opt. Phys.* **2017**, *50*, 123001. [[CrossRef](#)]
15. Pindzola, M.S.; Robicieux, F.; Colgan, J. Electron-impact ionization of  $H_2^+$  using a time-dependent close-coupling method. *J. Phys. B At. Mol. Opt. Phys.* **2005**, *38*, L285. [[CrossRef](#)]
16. Kim, Y.K.; Rudd, M.E. Binary-encounter-dipole model for electron-impact ionization. *Phys. Rev. A* **1994**, *50*, 3954. [[CrossRef](#)]
17. Deutsch, H.; Becker, K.; Matt, S.; Märk, T.D. Theoretical determination of absolute electron-impact ionization cross sections of molecules. *Int. J. Mass Spectrom.* **2000**, *197*, 37. [[CrossRef](#)]
18. Khare, S.P. *Introduction to the Theory of Collisions of Electrons with Atoms and Molecules*; Physics of Atoms and Molecules Series; Springer: New York, NY, USA, 2001.
19. Kumar, Y.; Kumar, M. Theoretical partial ionization cross sections by electron impact for production of cations from  $CH_3OH$ ,  $CO_2$  and  $NH_3$ . *Chem. Phys. Lett.* **2020**, *740*, 137071. [[CrossRef](#)]
20. Pal, S.; Kumar, J.; Märk, T.D. Differential, partial and total electron impact ionization cross sections for  $SF_6$ . *J. Chem. Phys.* **2004**, *120*, 4658. [[CrossRef](#)]
21. Pal, S.; Kumar, N. Electron-Collision-Induced Dissociative Ionization Cross Sections for Silane. *Adv. Phys. Chem.* **2009**, 309292. [[CrossRef](#)]
22. Tanaka, H.; Brunger, M.J.; Campbell, L.; Kato, H.; Hoshino, M.; Rau, A.R.P. Scaled plane-wave Born cross sections for atoms and molecules. *Rev. Mod. Phys.* **2016**, *88*, 025004. [[CrossRef](#)]
23. Graves, V.; Cooper, B.; Tennyson, J. The efficient calculation of electron impact ionization cross sections with effective core potentials. *J. Chem. Phys.* **2021**, *154*, 114104. [[CrossRef](#)]
24. Kim, Y.K.; Santos, J.P.; Parentea, F. Extension of the binary-encounter-dipole model to relativistic incident electrons. *Phys. Rev. A* **2000**, *62*, 052710. [[CrossRef](#)]
25. Ali, M.A.; Kim, Y.-K. Ionization cross sections by electron impact on halogen atoms, diatomic halogen and hydrogen halide molecules. *J. Phys. B At. Mol. Opt. Phys.* **2008**, *41*, 145202. [[CrossRef](#)]
26. Graves, V.; Cooper, B.; Tennyson, J. Calculated electron impact ionisation fragmentation patterns. *J. Phys. B At. Mol. Opt. Phys.* **2021**, *54*, 235203. [[CrossRef](#)]
27. Fedus, K.; Karwasz, G.P. Electron scattering on molecules: search for semi-empirical indications. *Eur. Phys. J. D* **2017**, *71*, 138. [[CrossRef](#)]
28. Hwang, W.; Kim, Y.-K.; Rudd, M.E. New model for electron-impact ionization cross sections of molecules. *J. Chem. Phys.* **1996**, *104*, 2956. [[CrossRef](#)]
29. Kim, Y.-K.; Hwang, W.; Weinberger, N.M.; Ali, M.A.; Rudd, M.E. Electron-impact ionization cross sections of atmospheric molecules. *J. Chem. Phys.* **1997**, *106*, 1026. [[CrossRef](#)]
30. Scott, G.E.; Irikura, K.K. Performance of binary-encounter-Bethe (BEB) theory for electron-impact ionization cross sections of molecules containing heavy elements ( $Z > 10$ ). *Surf. Interface Anal.* **2005**, *37*, 973. [[CrossRef](#)]
31. Irikura, K.K.; Ali, M.A.; Kim, Y.-K. Electron-impact total ionization cross-sections of the chlorofluoromethanes. *Int. J. Mass Spectrom.* **2003**, *222*, 189. [[CrossRef](#)]
32. Vriens, L. Electron exchange in binary encounter collision theory. *Proc. Phys. Soc. Lond.* **1966**, *89*, 13. [[CrossRef](#)]

33. Kim, Y.-K.; Irikura, K.K.; Ali, M.A. Electron-impact total ionization cross sections of molecular ions. *J. Res. Natl. Inst. Stand. Technol.* **2000**, *105*, 285. [[CrossRef](#)]
34. Irikura, K.K.; Kim, Y.-K.; Ali, M.A. Electron-impact total ionization cross sections of hydrocarbon ions. *J. Res. Natl. Inst. Stand. Technol.* **2002**, *107*, 63. [[CrossRef](#)]
35. Huo, W.M.; Kim, Y.-K. Use of relativistic effective core potentials in the calculation of total electron-impact ionization cross-sections. *Chem. Phys. Lett.* **2000**, *319*, 576. [[CrossRef](#)]
36. Gupta, D.; Choi, H.; Song, M.; Karwasz, G.P.; Yoon, J.-S. Electron impact ionization cross section studies of  $C_2F_x$  ( $x = 1-6$ ) and  $C_3F_x$  ( $x = 1-8$ ) fluorocarbon species. *Eur. Phys. J. D* **2017**, *71*, 88. [[CrossRef](#)]
37. Gupta, D.; Choi, H.; Singh, S.; Modal, P.; Antony, B.; Kwon, D.; Song, M.; Yoon, J.-S. Total Ionisation Cross sections of cyclic organic molecules. *J. Chem. Phys.* **2019**, *150*, 064313. [[CrossRef](#)]
38. Huber, S.E.; Mauracher, A.; Siiß, D.; Sukuba, I.; Urban, J.; Dmitry, D.; Probst, M. Total and partial electron impact ionization cross sections of fusion-relevant diatomic molecules. *J. Chem. Phys.* **2019**, *150*, 024306. [[CrossRef](#)] [[PubMed](#)]
39. Goswami, K.; Luthra, M.; Bharadvaja, A.; Arora, A.K.; Baluja, K.L. Electron impact partial ionization cross sections of 1-butanol. *Eur. Phys. J. D* **2022**, *76*, 97. [[CrossRef](#)]
40. Johnson, R.D., III. (Ed.) Computational Chemistry Comparison and Benchmark Database, NIST Standard Reference Database Number 101, Release 21, August 2020. Available online: <http://cccbdb.nist.gov/> (accessed on 20 March 2022).
41. GAUSSIAN 03; Gaussian, Inc.: Wallingford, UK, 2003.
42. Irikura, K.K. Semi-empirical estimation of ion-specific cross sections in electron ionization of molecules. *J. Chem. Phys.* **2016**, *145*, 224102. [[CrossRef](#)] [[PubMed](#)]
43. Swain, R.; Vasisht, G.; Tinetti, G. The presence of methane in the atmosphere of an extrasolar planet. *Nature* **2008**, *452*, 329. [[CrossRef](#)] [[PubMed](#)]
44. Mahaffy, R. Intensive Titan exploration begins. *Science* **2005**, *308*, 969. [[CrossRef](#)]
45. Tian, C.C.; Vidal, C.R. Cross sections of the electron impact dissociative ionization of CO, CH<sub>4</sub> and C<sub>2</sub>H<sub>2</sub>. *J. Phys. B* **1998**, *31*, 895. [[CrossRef](#)]
46. Lindsay, B.G.; Rejoub, R.; Stebbings, R.F. Production of positive ion pairs by electron-impact ionization of CH<sub>4</sub>. *J. Chem. Phys.* **2001**, *114*, 10225. [[CrossRef](#)]
47. Gadoum, A.; Benyoucef, D. Set of the electron collision cross sections for methane molecule. *IEEE Trans. Plasma Sci.* **2019**, *47*, 1505. [[CrossRef](#)]
48. Song, M.-Y.; Yoon, J.; Cho, H.; Itikawa, Y.; Karwasz, G.P.; Kokoouline, V.; Nakamura, Y.; Tennyson, J. Cross sections for electron collisions with methane. *J. Phys. Chem. Ref. Data* **2015**, *44*, 023101. [[CrossRef](#)]
49. Lindsay, B.G.; Mangan, M.A. *Interactions of Photons and Electrons with Molecules*; Landolt-Boörnstein: Numerical Data and Functional Relationships in Science and Technology—New Series, Group I: Elementary Particles, Nuclei and Atoms; Martienssen, W., Ed.; Springer: Berlin/Heidelberg, Germany; New York, NY, USA, 2003; Volume 17C, p. 5001.
50. Straub, C.; Lin, D.; Lindsay, B.G.; Smith, K.A.; Stebbings, R.F. Absolute partial cross sections for electron-impact ionization of CH<sub>4</sub> from threshold to 1000 eV. *Chem. Phys.* **1997**, *106*, 4430. [[CrossRef](#)]
51. NIST Chemistry WebBook, NIST Standard Reference Database Number 69. Available online: <https://webbook.nist.gov/chemistry/> (accessed on February 2022).
52. Goswami, K.; Luthra, M.; Arora, A.K.; Bharadvaja, A.; Baluja, K.L. Electron-impact cross sections of acetylene up to 5 keV. *Eur. Phys. J. D* **2022**, *76*, 94. [[CrossRef](#)]
53. Nixon, K.L.; Pires, W.A.D.; Neves, R.F.C.; Duque, H.V.; Jones, D.B.; Brunger, M.J.; Lopes, M.C.A. Electron impact ionisation and fragmentation of methanol and ethanol. *Int. J. Mass Spectrom.* **2016**, *404*, 48. [[CrossRef](#)]
54. Arora, A.K.; Gupta, K.K.; Goswami, K.; Bharadvaja, A.; Baluja, K.L. A binary-encounter-Bethe approach to compute electron-impact partial ionization cross sections of plasma relevant molecules such as hexamethyldisiloxane and silane. *Plasma Sour. Sci. Technol.* **2022**, *31*, 015008. [[CrossRef](#)]
55. Adamczyk, B.; Boerboom, A.J.H.; Schram, B.L.; Kistemaker, J. Partial ionization cross sections of He, Ne, H<sub>2</sub>, and CH<sub>4</sub> for electrons from 20 to 500 eV. *Chem. Phys.* **1966**, *44*, 4640. [[CrossRef](#)]
56. Orient, J.; Srivastava, S.K. Electron impact ionisation of H<sub>2</sub>O, CO, CO<sub>2</sub> and CH<sub>4</sub>. *J. Phys. B At. Mol. Opt. Phys.* **1987**, *20*, 3923. [[CrossRef](#)]
57. Chatham, H.; Hills, D.; Robertson, R.; Gallagher, A. Total and partial electron collisional ionization cross sections for CH<sub>4</sub>, C<sub>2</sub>H<sub>6</sub>, SiH<sub>4</sub>, and Si<sub>2</sub>H<sub>6</sub>. *J. Chem. Phys.* **1984**, *81*, 1770. [[CrossRef](#)]
58. Tarnovsky, V.; Levin, A.; Deutsch, H.; Becker, K. Electron impact ionization of CD<sub>x</sub> ( $x = 1-4$ ). *J. Phys. B At. Mol. Opt. Phys. Phys.* **1996**, *29*, 139. [[CrossRef](#)]
59. Janev, R.K.; Reiter, D. Collision processes of CH<sub>y</sub> and CH<sub>y</sub><sup>+</sup> hydrocarbons with plasma electrons and protons. *Phys. Plasmas* **2002**, *9*, 4071. [[CrossRef](#)]
60. Lindsay, G.; Mangan, M. *Landolt-Boörnstein Group I: Elementary Particles Nuclei and Atoms*; Springer: Berlin/Heidelberg, Germany; New York, NY, USA, 2003; pp. 1–5.
61. Bernath, P.F. The spectroscopy of water vapour: Experiment, theory and applications. *Phys. Chem. Chem. Phys.* **2002**, *4*, 1501. [[CrossRef](#)]
62. Larsson, M.; Geppert, W.D.; Nyman, G. Ion chemistry in space. *Rep. Prog. Phys.* **2012**, *75*, 066901. [[CrossRef](#)]

63. Savin, D.W.; Brickhouse, N.S.; Cowan, J.J.; Drake, R.P.; Federman, S.R.; Ferland, G.J.; Frank, A.; Gudipati, M.S.; Haxton, W.C.; Herbst, E.; Profumo, S.; et al. The impact of recent advances in laboratory astrophysics on our understanding of the cosmos. *Rep. Prog. Phys.* **2012**, *75*, 036901. [[CrossRef](#)] [[PubMed](#)]
64. Hobbie, R.K.; Roth, B.J. *Intermediate Physics for Medicine and Biology*; Springer: New York, NY, USA, 2007.
65. Byakov, V.M.; Stepanov, S.V. The mechanism for the primary biological effects of ionizing radiation. *Phys. Usp.* **2006**, *49*, 469. [[CrossRef](#)]
66. Liu, D.X.; Bruggeman, P.; Iza, F.; Rong, M.Z.; Kong, M.G. Global model of low-temperature atmospheric-pressure He + H<sub>2</sub>O plasmas. *Plasma Sources Sci. Technol.* **2010**, *19*, 025018. [[CrossRef](#)]
67. Tas, M.A.; van Veldhuizen, E.M.; Rutgers, W.R. Water is an active matrix of life for cell and molecular biology. *J. Phys. D* **1997**, *30*, 1636. [[CrossRef](#)]
68. Uehara, S.; Nikjoo, H.; Goodhead, D.T. Comparison and Assessment of Electron Cross Sections for Monte Carlo Track Structure Codes. *Rad. Res.* **1999**, *152*, 202. [[CrossRef](#)]
69. Kovtun, Y.V. Mean energy of water molecule ionization by electron impact. *Technol. Phys.* **2015**, *60*, 1110. [[CrossRef](#)]
70. Straub, H.C.; Lindsay, B.G.; Smith, K.A.; Stebbings, R.F. Absolute partial cross sections for electron-impact ionization of H<sub>2</sub>O and D<sub>2</sub>O from threshold to 1000 eV. *J. Chem. Phys.* **1998**, *108*, 109. [[CrossRef](#)]
71. Sahlaoui, M.; Bouamoud, M. Cross sections for electron-impact ionization of water molecules. *Can. J. Phys.* **2011**, *89*, 723. [[CrossRef](#)]
72. Champion, C.; Hanssen, J.; Hervieux, P.A. Electron impact ionization of water molecule. *J. Chem. Phys.* **2002**, *117*. [[CrossRef](#)]
73. Zavilopulo, A.N.; Chipev, F.F.; Shpenik, O.B. Ionization of water and carbon dioxide molecules by electron impact near threshold. *Nuc. Instru. Meth. Phys. Res. B* **2005**, *233*, 298. [[CrossRef](#)]
74. Song, M.-Y.; Cho, H.; Karwasz, G.P.; Kokoouline, V.; Nakamura, Y.; Tennyson, J.; Faure, A.; Mason, N.J.; Itikawa, Y. Cross Sections for Electron Collisions with H<sub>2</sub>O. *J. Phys. Chem. Ref. Data* **2021**, *50*, 023103. [[CrossRef](#)]
75. Itikawa, Y.; Mason, N. Cross sections for electron collisions with water molecules. *J. Phys. Chem. Ref. Data* **2005**, *34*, 1. [[CrossRef](#)]
76. King, S.J.; Price, S.D. Electron ionization of H<sub>2</sub>O. *Int. J. Mass Spectrom.* **2008**, *277*, 84. [[CrossRef](#)]
77. Montenegro, E.C.; Scully, S.W.J.; Wyer, J.A.; Senthil, V.; Shah, M.B. Evaporation, fission and auto-dissociation of doubly charged water. *J. Electron. Spectrosc. Relat. Phenom.* **2007**, *155*, 81. [[CrossRef](#)]
78. Cromer, D.T.; Ryan, R.R.; Schiferl, D. The structure of nitromethane at pressures of 0.3 to 6.0 GPa. *J. Phys. Chem.* **1989**, *89*, 2315. [[CrossRef](#)]
79. Zhang, Y.X.; Bauer, S.H. Modeling the Decomposition of Nitromethane, Induced by Shock Heating. *J. Phys. Chem. B* **1997**, *101*, 8717. [[CrossRef](#)]
80. Winey, J.M.; Gupta, Y.M. Shock-Induced Chemical Changes in Neat Nitromethane: Use of Time-Resolved Raman Spectroscopy. *J. Phys. Chem. B* **1997**, *101*, 10733. [[CrossRef](#)]
81. Winey, J.M.; Gupta, Y.M. UV-Visible Absorption Spectroscopy to Examine Shock-Induced Decomposition in Neat Nitromethane. *J. Phys. Chem. A* **1997**, *101*, 9333. [[CrossRef](#)]
82. Bouyer, V.; Darbord, I.; Herve, P.; Baudin, G.; Gallic, C.L.; Clement, F.; Chavent, G. Shock-to-Detonation Transition of Nitromethane: Time-Resolved Emission Spectroscopy Measurements. *Combust. Flame* **2006**, *144*, 139. [[CrossRef](#)]
83. Gruzdkov, Y.A.; Gupta, Y.M. Emission and Fluorescence Spectroscopy To Examine Shock-Induced Decomposition in Nitromethane. *J. Phys. Chem.* **1998**, *102*, 8325. [[CrossRef](#)]
84. Kelzenberg, S.; Eisenreich, N.; Eckl, W.; Weiser, V. Modelling Nitromethane Combustion. *Propellants Explos. Pyrotech.* **1999**, *24*, 189. [[CrossRef](#)]
85. Boyer, E.; Kuo, K.K. Modeling of Nitromethane Flame Structure and Burning Behavior. *Proc. Combust. Inst.* **2007**, *31*, 2045. [[CrossRef](#)]
86. Brill, T.B.; James, K.J. Kinetics and mechanisms of thermal decomposition of nitroaromatic explosives. *Chem. Rev.* **1993**, *93*, 2667. [[CrossRef](#)]
87. Zhang, Q.; Li, W.; Lin, D.C.; He, N.; Duan, Y. Influence of Nitromethane Concentration on Ignition Energy and Explosion Parameters in Gaseous Nitromethane/Air Mixtures. *J. Hazard Mater.* **2011**, *185*, 756. [[CrossRef](#)]
88. Burger, A.; Parulkar, A.P. Relationships between chemical structure and biological activity. *Annu. Rev. Pharmacol.* **1966**, *6*, 19. [[CrossRef](#)]
89. Kasemo, B. Biological surface science. *Surf. Sci.* **2002**, *500*, 656. [[CrossRef](#)]
90. Jiao, C.Q.; DeJoseph, C.A., Jr.; Garscadden, A. Formation of Positive and Negative Ions in CH<sub>3</sub>NO<sub>2</sub>. *J. Phys. Chem. A* **2003**, *107*, 9040. [[CrossRef](#)]
91. Kandel, R.J. Appearance Potential Studies. II. Nitromethane. *J. Chem. Phys.* **1955**, *23*, 84. [[CrossRef](#)]
92. Hamilton, J.R.; Tennyson, J.; Huang, S.; Kushner, M.J. Calculated cross sections for electron collisions with NF<sub>3</sub>, NF<sub>2</sub> and NF with applications to remote plasma sources. *Plasma Sources Sci. Technol.* **2017**, *26*, 065010. [[CrossRef](#)]
93. Barnard, G.P. *Modern Mass Spectrometry*; Institute of Physics: London, UK, 1953.
94. Ausloos, P.; Clifton, C.L.; Lias, S.G.; Mikaya, A.I.; Stein, S.E.; Tchekhovskoi, D.V.; Sparkman, O.D.; Zaikin, V.; Zhu, D. The critical evaluation of a comprehensive mass spectral library. *J. Am. Soc. Mass Spectrom.* **1999**, *10*, 287. [[CrossRef](#)]